Impedance Modeling and Stability Analysis of Dual Active Bridge Converter with LC Input Filter

Fan Feng, *Student Member*, *IEEE*, Xin Zhang, *Member*, *IEEE*, Fanfan Lin, and Hoay Beng Gooi, *Senior Member*, *IEEE*

(Invited)

***Abstract*—The dual active bridge (DAB) converter is gaining more and more attention in various applications such as energy storage systems, electric vehicles and smart grids. To improve the quality of the input current, a LC filter is often cascaded at the input side of the DAB converter. However, there are instable problems of this cascaded system due to the impedance interactions of the DAB converter and the LC filter, although the DAB converter is stable at the individual operation mode. To assess the stability of the cascaded system of the DAB converter and the LC filter, the impedance model of the DAB converter is firstly developed based on generalized state-space averaging method. The developed impedance model can be used to accurately predict the stability of the DAB converter with its LC input filter. Based on the stability analysis, the optimum filter parameter design guideline is determined. The impedance model and stability analysis are validated by the simulation and experimental results.**

***Index Terms*—Dual active bridge, generalized state-space averaging, stability analysis, phase-shift modulation.**

I. Introduction

THE bidirectional dc-dc converters have greatly increased in popularity with the rapid expansion of uninterruptible power supply systems, distributed resources interface, electric vehicles and the energy storage systems. Compared to other traditional bidirectional buck/boost converters, the dual active bridge (DAB) converter is becoming more and more popular because of its advantages such as the high power density, soft switching properties, galvanic isolation and less passive components. Fig. 1 shows the circuit topology of the DAB converter cascaded with the LC filter, which is used to improve the input current quality of the DAB converter. The battery is connected to the output side of the DAB converter. By regulating the transformer current of the DAB converter, the shift between the charging and discharging mode of the battery can be achieved.

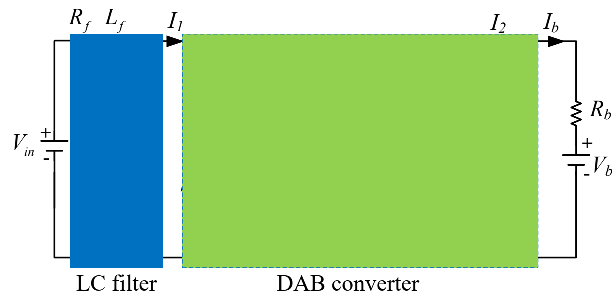

Fig.1. circuit topology of the DAB converter with its LC filter.

However, although the DAB converter is stable when operating individually, the dc-link voltage may become oscillating when the LC filter is cascaded with the DAB converter due to poor design of the circuit parameters. The stability issues have also been found in other dc and ac cascaded systems [9-13]. To investigate the stability issue in cascaded systems, the impedance based stability criterion was first proposed by Middlebrook in [14], implying that the stability of the cascaded converter must take the impedance interaction into consideration, and the required input impedance should be far greater than the output impedance of cascaded filter. Based on the impedance of the converters, some improved stability criteria with the concept of the forbidden region are proposed in [15, 16]. It is found that the minor loop gain, which is the ratio of the source output impedance to the load input impedance, should satisfy the Nyquist criterion to ensure the stability of the cascaded system [17, 18].

Therefore, to apply the above-mentioned stability criteria, the closed-loop impedance models are necessary for the stability analysis of the cascaded systems [10, 19, 20]. However, because the transformer current is pure ac, the traditional state-space averaging (SSA) method cannot be applied to the modeling of the DAB converter [21, 22]. The reduced-order impedance models of the DAB converter are derived in [7, 23], neglecting the dynamics of the transformer current. Based on the concept of the dynamic phasor, a generalized model is proposed in [24] and shows more accuracy than reduced-order models [25]. But this model is not extended to the derivation of

Manuscript was submitted for review on 14, September, 2018.

Fan Feng is currently pursuing the Ph. D degree from the School of Electrical and Electronic Engineering, Nanyang Technological University(email: FFENG003@e.ntu.edu.sg).

Xin Zhang is an Assistant Professor at the School of Electrical and Electronic Engineering of Nanyang Technological University(email: jackzhang@ntu.edu.sg).

Fanfan Lin is now pursuing her Ph.D. degree in the School of Electrical and Electronic Engineering, NTU(email: FANFAN001@e.ntu.edu.sg).

Hoay Beng Gooi is with the School of Electrical and Electronic Engineering, Nanyang Technological University(email: EHBGOOI@ntu.edu.sg).

Digital Object Identifier 10.30941/CESTEMS.2018.00036

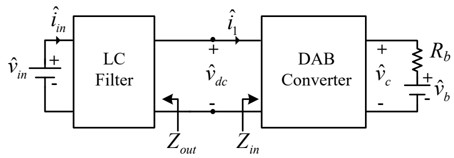

Fig. 2. Small-signal model of cascaded system.

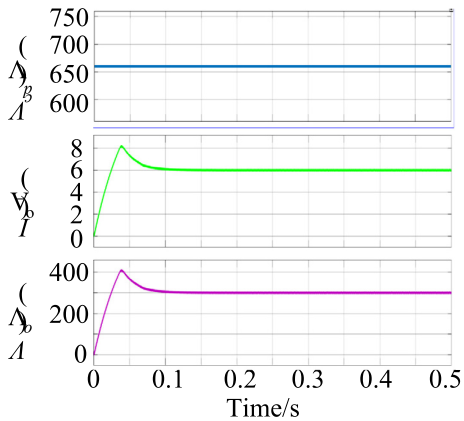

Fig. 3. Waveforms of the DAB converter without an LC filter.

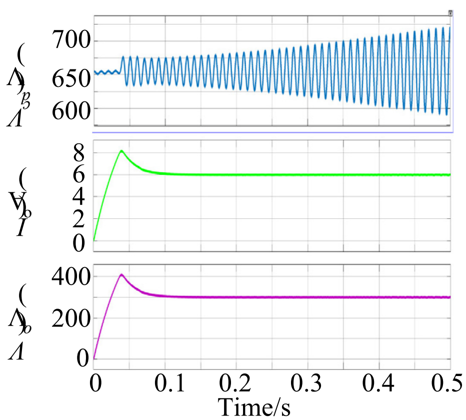

Fig. 4. Waveforms of the cascaded system.

the DAB closed-loop impedances. Moreover, the stability of the DAB converter with its LC input filter has not yet been analyzed.

To fill up this gap, the impedance of the DAB converter is developed in this paper based on the concept of dynamic phasor. The leakage inductance current and the resonant transition intervals are taken into consideration in the impedance model, thus enabling the dynamics to be studied and improving accuracy. The stability of the DAB converter with its LC input filter is analyzed. For the stability consideration, the optimum parameters of the LC filter are also provided.

The rest of the paper is organized as follows: Section II describes the instability phenomenon when the DAB converter is cascaded with a LC filter, and Section III shows the derivation of a full-order continuous-time average model for the DAB converter and the small-signal control-to-output transfer function through GSSA to obtain the converter input impedance. In section IV, the stability of the cascaded system consisting of the DAB converter and a LC input filter is assessed. Section V verifies the theory through experimental results. The conclusion will be summarized in Section VI.

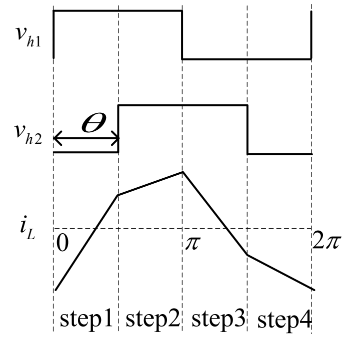

Fig. 5. Operating waveforms of the DAB converter in one switching cycle.

II. Instability Phenomenon Description

The cascaded system of the DAB converter and the LC filter can be interpreted by the small signal model shown in Fig. 2.

The LC filter is aimed to decrease the load current fluctuations so as to improve the quality of the input current for the DAB converter. However, the stability of the cascaded system can be degraded due to the mismatch of the output impedance of the LC filter and the input impedance of the DAB converter. When the DAB converter is operating individually the waveforms of the dc-link voltage V_{dc}, output current I_o and output voltage V_o are shown in Fig. 3. As can be seen from Fig. 3, the DAB converter is operating stably. However, when the input LC filter is cascaded with the DAB converter, as shown in Fig. 4, the dc-link voltage V_{dc} is oscillating and diverging, indicating that the cascaded system is no longer stable.

What should be emphasized is that for stability analysis, this paper only focuses on the forward interactions of the input impedance and other converters, excluding the reverse interaction. According to [7], different power flow direction gives rise to different impedance interaction and it is more stable in the reverse direction (battery discharging) than in the forward direction (battery charging).

III. Full-order Model of DAB Converters

As shown in Fig. 1, the DAB converter consists of two full-bridge on both the primary and secondary sides of the high-frequency transformer. The transformer here matches the voltage difference between the two sides and provides galvanic isolation. And the leakage inductance of the transformer serves as the energy storage element. By adjusting the phase shift between the output voltages of the two H-bridges, the direction and magnitude of the transferred power in the DAB converter can be controlled.

To realize the phase shift of the output voltages, three modulation strategies can be used. The first one is the single phase-shifted (SPS) modulation, which generates square wave of 50% duty ratio for each bridge. The average power transferred is adjusted by the phase-shift angle of the two bridges. The second one is the dual phase-shifted (DPS) control, in which two bridges generates three-level voltage and the inner phase shift ratios in two bridges are the same. The last modulation strategy is the triple phase-shifted control (TPS), which adds one more angle to be modulated on the basis of DPS. In other words, the inner phase shift ratios of two bridges are different from each other. This paper focuses on the stability analysis of the DAB converter with its LC input filter. So the most commonly used SPS modulation method is adopted. Fig.5 describes the operating waveforms of the SPS method. θ is the phase shift between the output voltages of the primary and secondary bridges: v_{h1} and v_{h2}. The impedance model of the DPS or TPS based DAB converter can also be derived with the similar derivation process.

A. Generalized averaging of the DAB converter

Because of the ac components in the transformer, the generalized state average modeling is adopted to set a continuous-time DAB model. In this method, the state variable, $x(\tau)$ is expressed by Fourier series terms at multiples of the converter switching frequency to represent the ac states during the period of one cycle [22].

$$x(\tau)=\sum_{k=-\infty}^{\infty}\langle x\rangle_k(t)e^{jkw_s\tau} \tag{1}$$

where $w_s=2\pi f_s$; f_s is the switching frequency of the DAB converter and $\langle x\rangle_k(t)$ is the coefficient in the Fourier series

$$\langle x\rangle_k(t)=\frac{1}{T}\int_{t-T}^{t}x(\tau)e^{-jkw_s\tau}d\tau \tag{2}$$

Applying more terms of the Fourier series will lead to a higher accuracy in modelling. In this paper, the model uses the first harmonic approximation, which includes the k = 0 and k = ±1 terms in the Fourier series decomposition.

From the operating waveforms shown in Fig. 5, the switching function at the input bridge, $s_1(\tau)$, is expressed as:

$$s_1(\tau)=\begin{cases}1, & 0\le\tau\le\dfrac{T}{2}\\ -1, & \dfrac{T}{2}\le\tau\le T\end{cases} \tag{3}$$

where $T=1/f_s$ and τ is a parameter representing the time.

From Fig. 5, the switching function at the output bridge, $s_2(\tau)$ is calculated as (4).

$$s_2(\tau)=\begin{cases}1, & \dfrac{dT}{2}\le\tau\le\dfrac{T}{2}+\dfrac{dT}{2}\\ -1, & 0\le\tau\le\dfrac{dT}{2}\,or\,\dfrac{T}{2}+\dfrac{dT}{2}\le\tau<T\end{cases} \tag{4}$$

where d is the phase shift ratio and satisfies $0 < d < 1$.

According to the equations of Fourier series decomposition, firstly we get the zeroth coefficients of $s_1(t)$ and $s_2(t)$ are both zero:

$$\langle s_1\rangle_0=\langle s_2\rangle_0=0 \tag{5}$$

And the first coefficient of $s_1(t)$ and $s_2(t)$ can also be derived as:

$$\langle s_1\rangle_1^R=0 \tag{6}$$

$$\langle s_1\rangle_1^I=-\frac{2}{\pi} \tag{7}$$

$$\langle s_2\rangle_1^R=-\frac{2\sin d\pi}{\pi} \tag{8}$$

$$\langle s_2\rangle_1^I=-\frac{2\cos d\pi}{\pi} \tag{9}$$

where the superscript R represents the real part of the complex variable; and the superscript I represents the imaginary part of the complex variable. And these rules apply in the whole paper.

The state equations of the DAB converter can be expressed as (10) and (11):

$$L\frac{di_L}{dt}=s_1V_{dc}-s_2V_c \tag{10}$$

$$C\frac{du_c}{dt}=s_2i_L-\frac{V_c-V_b}{R_b} \tag{11}$$

And the input current i_1 and output current i_b can be expressed by the forgoing parameters:

$$i_1=s_1i_L \tag{12}$$

$$i_b=\frac{V_c-V_b}{R_b} \tag{13}$$

The ac ripples of dc variables can be neglected. So only the zeroth coefficient of v_c and v_{dc} are considered in the state equations. Likewise, due to the pure ac characteristics of i_L the k = ±1 terms in the Fourier series of i_L are included in the state equations. By means of the multifrequency averaging method in [26], the derivative of the zeroth coefficient and the first coefficient of state variables, i_L and v_c in (10) and (11) can be derived and organized in matrix form as (14):

$$\frac{d}{dt}\begin{bmatrix}\langle v_c\rangle_0\\ \langle i_L\rangle_1^R\\ \langle i_L\rangle_1^I\end{bmatrix}=\begin{bmatrix}-\dfrac{1}{CR_b} & \dfrac{2\langle s_2\rangle_1^R}{C} & \dfrac{2\langle s_2\rangle_1^I}{C}\\ -\dfrac{\langle s_2\rangle_1^R}{L} & 0 & w_s\\ -\dfrac{\langle s_2\rangle_1^I}{L} & -w_s & 0\end{bmatrix}\begin{bmatrix}\langle v_c\rangle_0\\ \langle i_L\rangle_1^R\\ \langle i_L\rangle_1^I\end{bmatrix}+\begin{bmatrix}0 & \dfrac{1}{CR_b}\\ \dfrac{\langle s_1\rangle_1^R}{nL} & 0\\ \dfrac{\langle s_1\rangle_1^I}{nL} & 0\end{bmatrix}\begin{bmatrix}V_{dc}\\ V_b\end{bmatrix} \tag{14}$$

Since the ac components of i_1 and i_b can be neglected, the dc component in i_1 and i_b in (12) and (14) can be also be achieved:

$$\begin{bmatrix}\langle i_1\rangle_0\\ \langle i_b\rangle_0\end{bmatrix}=\begin{bmatrix}0 & 2n\langle s_1\rangle_1^R & 2n\langle s_1\rangle_1^I\\ \dfrac{1}{R_b} & 0 & 0\end{bmatrix}\begin{bmatrix}\langle v_c\rangle_0\\ \langle i_L\rangle_1^R\\ \langle i_L\rangle_1^I\end{bmatrix}+\begin{bmatrix}0 & 0\\ 0 & \dfrac{-1}{R_b}\end{bmatrix}\begin{bmatrix}V_{dc}\\ V_b\end{bmatrix} \tag{15}$$

B. Impedance modelling of the DAB converter

The open-loop small signal model of the DAB converter is obtained by applying perturbation to the average model shown

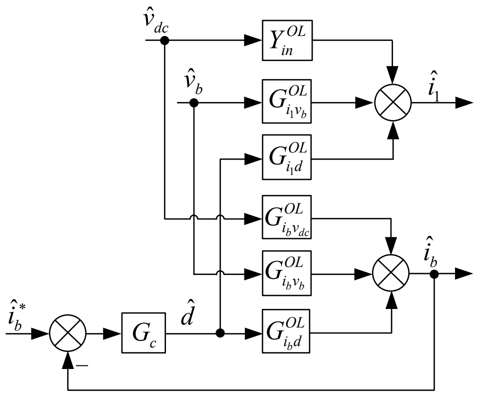

Fig. 6. Small-signal block diagram of the DAB converter.

in (14) and (15). The uppercase letters represent the steady state values of the variables and $\hat{x}$ represents the small signal value of the variable x. The resulting matrix equations are expressed as (16) and (17).

$$\frac{\mathrm{d}}{\mathrm{d}t}\begin{bmatrix}\langle\hat v_c\rangle_0\\ \langle\hat i_L\rangle_1^R\\ \langle\hat i_L\rangle_1^I\end{bmatrix}=\begin{bmatrix}-\frac{1}{CR_b} & \frac{2\langle s_2\rangle_1^R}{C} & \frac{2\langle s_2\rangle_1^I}{C}\\ -\frac{\langle s_2\rangle_1^R}{L} & 0 & w_s\\ -\frac{\langle s_2\rangle_1^I}{L} & -w_s & 0\end{bmatrix}\begin{bmatrix}\langle\hat v_c\rangle_0\\ \langle\hat i_L\rangle_1^R\\ \langle\hat i_L\rangle_1^I\end{bmatrix}$$
$$+\begin{bmatrix}0 & \frac{2}{C}((\langle i_L\rangle_1^R\frac{\partial\langle s_2\rangle_1^R}{\partial d}+\langle i_L\rangle_1^I\frac{\partial\langle s_2\rangle_1^I}{\partial d}) & \frac{1}{CR_b}\\ \frac{\langle s_1\rangle_1^R}{nL} & \frac{V_{dc0}}{nL}\frac{\partial\langle s_1\rangle_1^R}{\partial d}-\frac{V_{c0}}{L}\frac{\partial\langle s_2\rangle_1^R}{\partial d} & 0\\ \frac{\langle s_1\rangle_1^I}{nL} & \frac{V_{dc0}}{nL}\frac{\partial\langle s_1\rangle_1^I}{\partial d}-\frac{V_{c0}}{L}\frac{\partial\langle s_2\rangle_1^I}{\partial d} & 0\end{bmatrix}\begin{bmatrix}\hat v_{dc}\\ \hat d\\ \hat v_b\end{bmatrix}\quad(16)$$

$$\begin{bmatrix}\hat i_1\\ \hat i_b\end{bmatrix}=\begin{bmatrix}0 & 2n\langle s_1\rangle_1^R & 2n\langle s_1\rangle_1^I\\ \frac{1}{R_b} & 0 & 0\end{bmatrix}\begin{bmatrix}\langle\hat v_c\rangle_0\\ \langle\hat i_L\rangle_1^R\\ \langle\hat i_L\rangle_1^I\end{bmatrix}$$
$$+\begin{bmatrix}0 & 2n\langle i_L\rangle_1^R\frac{\partial\langle s_1\rangle_1^R}{\partial d}+2n\langle i_L\rangle_1^I\frac{\partial\langle s_1\rangle_1^I}{\partial d} & 0\\ 0 & 0 & -\frac{1}{R_b}\end{bmatrix}\begin{bmatrix}\hat v_{dc}\\ \hat d\\ \hat v_b\end{bmatrix}\quad(17)$$

The battery current is measured for the control of the DAB converter. The small signal control block diagram of the output current regulation is shown in Fig. 6. The open-loop transfer functions. Y_{in}^{OL}, $G_{i_1v_b}^{OL}$, $G_{i_1d_1}^{OL}$, $G_{i_bv_{dc}}^{OL}$, $G_{i_bv_b}^{OL}$ and $G_{i_bd_1}^{OL}$, defined in (18), can be calculated using MATLAB based on the small signal model (17) and (18). The current controller G_c is expressed as $G_c = k_p + k_i/s$. k_p and k_i are the proportional and integral coefficients of the controller.

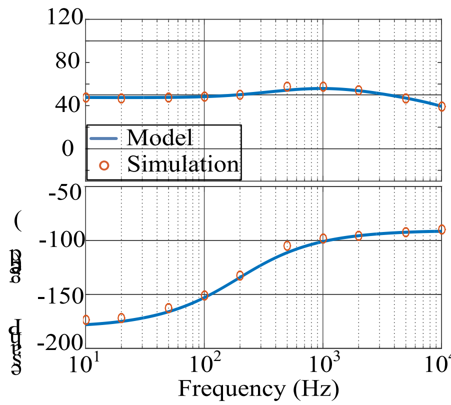

Fig. 7. Bode plots of the open-loop input impedances.

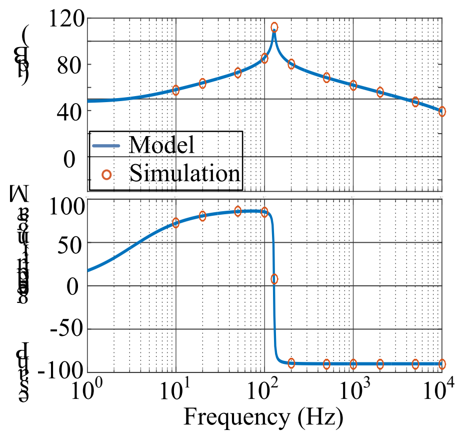

Fig. 8. Bode plots of the closed-loop input impedances.

TABLE I
PARAMETERS FOR SIMULATION

Symbols	PARAMETERS	Values
R_b	load of the DAB converter	25Ω
n	turns ratio of the transformer	2
D	phase-shift ratio of the first H bridge	0.5
I_l	rated inductor current in the DAB converter	38.82A
C	DC side output filter capacitance	600μF
L	DC inductor	100uH
K_p	proportional coefficient of the current controller	1
K_i	integral coefficient of the current controller	80
f_s	switching frequency of the DAB converter	20kHz
V_{dc}	input voltage of the DAB converter	660V
V_b	output voltage of the DAB converter	300V

$$\begin{bmatrix}\hat i_1\\ \hat i_b\end{bmatrix}=\begin{bmatrix}Y_{in}^{OL} & G_{i_1d}^{OL} & G_{i_1v_b}^{OL}\\ G_{i_bv_{dc}}^{OL} & G_{i_bd}^{OL} & G_{i_bv_b}^{OL}\end{bmatrix}\begin{bmatrix}\hat v_{dc}\\ \hat d\\ \hat v_b\end{bmatrix}\quad(18)$$

The close-loop admittance Y_{in}^{CL} of the DAB converter could be derived on the basis of the block diagram as follows:

$$Y_{in}^{CL}=\frac{\hat i_1}{\hat v_{dc}}=(Y_{in}^{OL}-\frac{G_cG_{i_bv_{dc}}^{OL}}{1+G_{i_bv_{dc}}^{OL}G_{i_bd_1}^{OL}})\quad(19)$$

So, the closed-loop impedance Z_{in}^{CL} can be calculated as (20).

$$Z_{in}^{CL}=\frac{1+G_{i_b v_{dc}}^{OL}G_{i_b d_1}^{OL}}{Y_{in}^{OL}\left(1+G_{i_b v_{dc}}^{OL}G_{i_b d_1}^{OL}\right)-G_c G_{i_b v_{dc}}^{OL}} \tag{20}$$

C. Verification of the impedance model

To verify the developed impedance model, a simulation model is built in MATLAB. The input impedance of the DAB converter is measured and compared with the bode plot of the model. The circuit and controller parameters of the DAB converter are listed in Table I.

The bode plots of the open-loop impedance of the DAB converter are shown in Fig. 7. The blue line denotes the model prediction. And the scatter plots mean the simulation measured results on certain frequencies. It is proven that in the open-loop situations, the simulation results match well with the impedance model derived in Section III.B.

Fig. 8 shows the closed-loop impedance of the DAB converter. As can be seen from Fig. 8, the simulation measured values also match very well with the prediction of the developed model. Hence, the open-loop and closed-loop measurements verify the correctness of the developed model.

IV. Stability Analysis of the Cascaded System

In the cascaded system of a LC filter and a DAB converter, since the control scheme keeps the same when the battery is charging or discharging, the source and load are well defined and do not change in operation. The equivalent circuit of this cascaded system is given in Fig. 9. Z_{out} is the output impedance of the LC filter and Z_{in} is the input impedance of DAB converter.

According to Fig. 9, the minor loop gain T_m of the cascaded system should be organized as:

$$T_m=\frac{Z_{out}}{Z_{in}} \tag{21}$$

Therefore, the cascaded system will turn out to be stable if T_m satisfies the Nyquist criterion.

According to [27], the output impedance of the LC filter is given as (22).

$$Z_{out}=\frac{sL_f+R_f}{s^2C_fL_f+sC_fR_f+1} \tag{22}$$

And the input impedance of the DAB converter has been given in section III.B.

To assess the stability of the cascaded, three groups of LC filters are selected for stability analysis. The LC filter parameters are given in Table II. The bode plots of Z_{out} and Z_{in} are drawn using MATLAB, shown in Fig. 10. As can be seen from Fig. 10, at the low frequencies, Z_{in} shows the negative resistance characteristics. Since the output impedance of the filter #1 and filter #2 both intersect with Z_{in} and their phase differences are larger than 180 degree. According to the Nyquist criterion, the cascaded system of the DAB converter with the filter #1 or filter #2 is not stable due to their impedance interactions.

As for the filter #3, the output impedance of the LC filter is

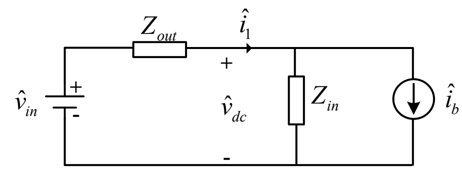

Fig. 9. The equivalent circuit of this cascaded system.

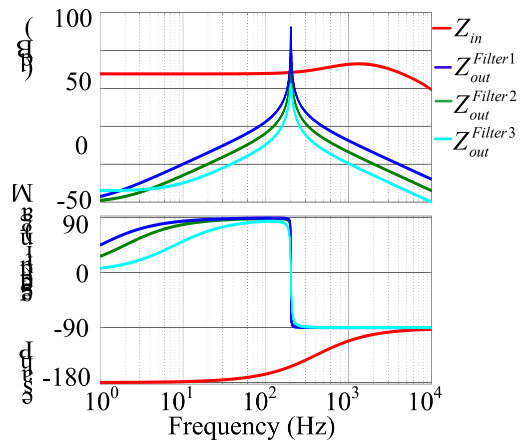

Fig. 10. Input filters and DAB converter for stability analysis.

TABLE II
Parameters for LC Filters

Parameters	Values
L_{f1}	0.00318 H
C_{f1}	0.0002 F
L_{f2}	0.00159 H
C_{f2}	0.0004 F
L_{f3}	0.0008 H
C_{f3}	0.0008 F

always smaller than Z_{in} within the whole frequency range. Therefore, the stability of the cascaded system is not degraded. For stability consideration, the filter #3 is preferred.

As can be seen in Fig. 10, the peak value of the magnitude of Z_{out} is increasing with the decreasing of the filter capacitance, which will lead to the impedance intersection with Z_{in}. Therefore, although the cost and volume of the filters need to be considered for the system design, a general conclusion can be inferred from the above analysis is that the value of the filter capacitance should be relatively large to ensure the stability of the cascaded system.

V. Experimental Results

The above analysis is further tested by the OPAL-RT based hardware-in-the-loop experiments. The circuit and controller parameters of the DAB converter are shown in Table I. The filter parameters are shown in Table II.

As shown in Fig. 11, the dc-link voltage is oscillating when the filter #1 is cascaded with the DAB converter. This is expected as the bode plots of the output impedance of the filter #1 intersects with Z_{in}. Moreover, the voltage is oscillating at 200 Hz, which is also the intersection frequency of the output impedance of filter #1 and Z_{in}. Therefore, the experimental results coincide with the analysis in section IV. The developed model is able to predict the instable problems of the DAB converter and its LC filter.

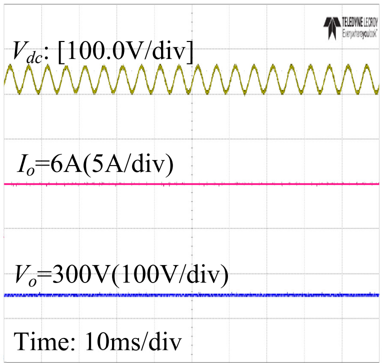

Fig. 11. The waveforms of the DAB converter with filter #1.

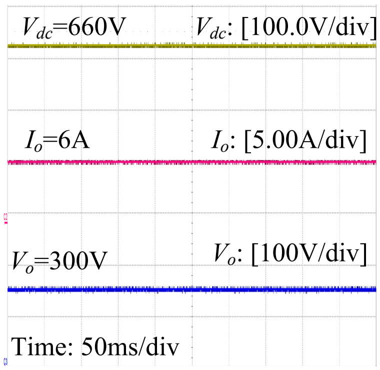

Fig. 12. The waveforms of the DAB converter with filter #3.

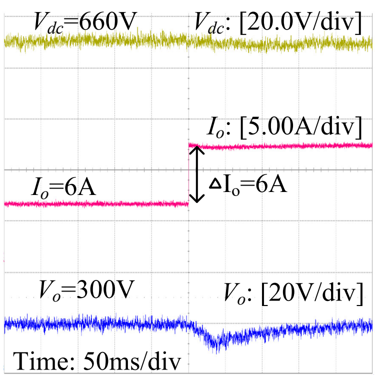

Fig. 13. The situation with a load step change.

To improve the stability of the cascaded system, the filter #1 is changed by the filter #3. The waveforms are shown in Fig. 12 As shown in Fig. 12, the dc-link voltage is no longer oscillating since the impedance of filter #3 is smaller than Z_{in} as shown in Fig. 10. The stability of the system is improved as the filter #3 is used. Because of the reduced output impedance of the LC filter, the stability margin of the cascaded system becomes larger. To test the dynamic performance of the filter, a load step change is applied to the system, the waveforms of the cascaded system are still stable as shown in Fig. 13. Therefore, the stability of the cascaded system is ensured when the filter #3 is cascaded with the DAB converter.

VI. Conclusion

The full-order impedance model of the DAB converter has been developed, which considers the ac components in the transformer current of the DAB converter. The open-loop and closed-loop impedance models have been both validated by simulation results. Based on the developed impedance model, the stability of the DAB converter with its LC input filter has been analyzed in detail. A general design guideline has also been provided for the stability consideration. The theoretical analysis has been validated by the experimental results.

References

[1] B. Zhao, Q. Song, W. Liu, and Y. Sun, "Overview of dual-active-bridge isolated bidirectional DC–DC converter for high-frequency-link power-conversion system," *IEEE Transactions on Power Electronics,* vol. 29, no. 8, pp. 4091-4106, 2014.

[2] N. M. L. Tan, T. Abe, and H. Akagi, "Design and performance of a bidirectional isolated DC–DC converter for a battery energy storage system," *IEEE Transactions on Power Electronics,* vol. 27, no. 3, pp. 1237-1248, 2012.

[3] C. Mi, H. Bai, C. Wang, and S. Gargies, "Operation, design and control of dual H-bridge-based isolated bidirectional DC–DC converter," *IET Power Electronics,* vol. 1, no. 4, pp. 507-517, 2008.

[4] F. Blaabjerg, Z. Chen, and S. B. Kjaer, "Power electronics as efficient interface in dispersed power generation systems," *IEEE transactions on power electronics,* vol. 19, no. 5, pp. 1184-1194, 2004.

[5] F. Blaabjerg, A. Consoli, J. A. Ferreira, and J. D. van Wyk, "The future of electronic power processing and conversion," *IEEE Transactions on Power Electronics,* vol. 20, no. 3, pp. 715-720, 2005.

[6] A. R. Alonso, J. Sebastian, D. G. Lamar, M. M. Hernando, and A. Vazquez, "An overall study of a Dual Active Bridge for bidirectional DC/DC conversion," in *Energy Conversion Congress and Exposition (ECCE), 2010 IEEE*, 2010, pp. 1129-1135: IEEE.

[7] Y. Tian, P. C. Loh, Z. Chen, F. Deng, and Y. Hu, "Impedance interactions in bidirectional cascaded converter," *IET Power Electronics,* vol. 9, no. 13, pp. 2482-2491, 2016.

[8] F. Krismer and J. W. Kolar, "Efficiency-optimized high-current dual active bridge converter for automotive applications," *IEEE Transactions on Industrial Electronics,* vol. 59, no. 7, pp. 2745-2760, 2012.

[9] X. Zhang, Q.-C. Zhong, and W.-L. Ming, "Stabilization of a cascaded dc converter system via adding a virtual adaptive parallel impedance to the input of the load converter," *IEEE Transactions on Power Electronics,* vol. 31, no. 3, pp. 1826-1832, 2016.

[10] P. Magne, B. Nahid-Mobarakeh, and S. Pierfederici, "Dynamic consideration of DC microgrids with constant power loads and active damping system—A design method for fault-tolerant stabilizing system," *IEEE Journal of Emerging and Selected Topics in Power Electronics,* vol. 2, no. 3, pp. 562-570, 2014.

[11] M. Wu and D. D.-C. Lu, "A novel stabilization method of LC input filter with constant power loads without load performance compromise in DC microgrids," *IEEE Transactions on Industrial Electronics,* vol. 62, no. 7, pp. 4552-4562, 2015.

[12] S. D. Sudhoff, K. Corzine, S. F. Glover, H. Hegner, and H. Robey, "DC link stabilized field oriented control of electric propulsion systems," *IEEE Transactions on Energy Conversion,* vol. 13, no. 1, pp. 27-33, 1998.

[13] S. Kelkar and F. Lee, "Stability analysis of a buck regulator employing input filter compensation," in *Power Electronics Specialists Conference, 1983 IEEE*, 1983, pp. 38-49: IEEE.

[14] R. Middlebrook and S. Cuk, "A general unified approach to modelling switching-converter power stages," in *Power Electronics Specialists Conference, 1976 IEEE*, 1976, pp. 18-34: IEEE.

[15] C. M. Wildrick, F. C. Lee, B. H. Cho, and B. Choi, "A method of defining the load impedance specification for a stable distributed power system," *IEEE Transactions on power Electronics,* vol. 10, no. 3, pp. 280-285, 1995.

[16] X. Feng, J. Liu, and F. C. Lee, "Impedance specifications for stable DC distributed power systems," *IEEE Transactions on Power Electronics,* vol. 17, no. 2, pp. 157-162, 2002.

[17] X. Zhang, X. Ruan, and K. T. Chi, "Impedance-based local stability criterion for dc distributed power systems," *IEEE Transactions on Circuits and Systems I: Regular Papers,* vol. 62, no. 3, pp. 916-925, 2015.

[18] J. Sun, "Impedance-based stability criterion for grid-connected inverters," *IEEE Transactions on Power Electronics,* vol. 26, no. 11, pp. 3075-3078, 2011.

[19] C. Zhao, S. D. Round, and J. W. Kolar, "Full-order averaging modelling of zero-voltage-switching phase-shift bidirectional DC–DC converters," *IET Power Electronics,* vol. 3, no. 3, pp. 400-410, 2010.

[20] A. M. Rahimi and A. Emadi, "Active damping in DC/DC power electronic converters: A novel method to overcome the problems of constant power loads," *IEEE Transactions on Industrial Electronics,* vol. 56, no. 5, pp. 1428-1439, 2009.

[21] F. Krismer and J. W. Kolar, "Accurate small-signal model for the digital control of an automotive bidirectional dual active bridge," *IEEE transactions on power electronics,* vol. 24, no. 12, pp. 2756-2768, 2009.

[22] K. Zhang, Z. Shan, and J. Jatskevich, "Large-and small-signal average-value modeling of dual-active-bridge DC–DC converter considering power losses," *IEEE Transactions on Power Electronics,* vol. 32, no. 3, pp. 1964-1974, 2017.

[23] Q. Ye, R. Mo, and H. Li, "Low-frequency resonance suppression of a Dual Active Bridge (DAB) DC/DC converter Enabled DC Microgrid with Constant Power Loads (CPLs) Based on Reduced-Order Impedance Models," *IEEE Journal of Emerging and Selected Topics in Power Electronics,* 2017.

[24] H. Qin and J. W. Kimball, "Generalized average modeling of dual active bridge DC–DC converter," *IEEE Transactions on Power Electronics,* vol. 27, no. 4, pp. 2078-2084, 2012.

[25] J. A. Mueller and J. W. Kimball, "Model-based determination of closed-loop input impedance for dual active bridge converters," in *Applied Power Electronics Conference and Exposition (APEC), 2017 IEEE*, 2017, pp. 1039-1046: IEEE.

[26] V. A. Caliskan, O. Verghese, and A. M. Stankovic, "Multifrequency averaging of DC/DC converters," *IEEE Transactions on Power Electronics,* vol. 14, no. 1, pp. 124-133, 1999.

[27] X. Zhang, X. Ruan, and Q.-C. Zhong, "Improving the stability of cascaded DC/DC converter systems via shaping the input impedance of the load converter with a parallel or series virtual impedance," *IEEE Transactions on Industrial Electronics,* vol. 62, no. 12, pp. 7499-7512, 2015.

Fan Feng (S' 18) received the B.S. and M. S. degrees in electrical engineering from Harbin Institute of Technology, Harbin, China, in 2011 and 2015, respectively. He is currently pursuing the Ph. D degree from the School of Electrical and Electronic Engineering, Nanyang Technological University, Singapore.

His research interests include the stability analysis of power electronic systems and active stabilization methods.

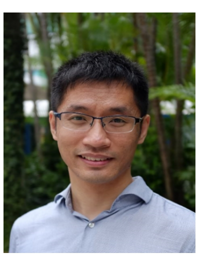

Xin Zhang (M'15) received the Ph.D. degree in Automatic Control and Systems Engineering from the University of Sheffield, U.K., in 2016 and the Ph.D. degree in Electronic and Electrical Engineering from Nanjing University of Aeronautics & Astronautics, China, in 2014. Currently, he is an Assistant Professor at the School of Electrical and Electronic Engineering of Nanyang Technological University. Dr Xin Zhang has received the highly-prestigious Chinese National Award for Outstanding Students Abroad at 2016. He is generally interested in power electronics, power system and advanced control theory, together with their applications in various sectors.

Fanfan Lin received the B.Sc. degree in School of Electrical Engineering and Automation from Harbin Institute of Technology, Harbin, China, in 2018. She is now pursuing her Ph.D. degree in the School of Electrical and Electronic Engineering, NTU.

Her research fixes on power converter design, including hybrid electromagnetic analysis, modern control theory, and modelling reducing technologies.

H. B. Gooi (SM'95) received the B.S. degree in electrical engineering from National Taiwan University, Taipei, Taiwan, in 1978; the M.S. degree in power engineering from the University of New Brunswick, Fredericton, NB, Canada, in 1980; and the Ph.D. degree in power engineering from the Ohio State University, Columbus, OH, USA, in 1983.

From 1983 to 1985, he was an Assistant Professor with the Department of Electrical Engineering, Lafayette College, Easton, PA, USA. From 1985 to 1991, he was a Senior Engineer with Empros (now Siemens), Minneapolis, MN, USA, where he was responsible for the design and testing coordination of domestic and international energy management system projects. In 1991, he joined the School of Electrical and Electronic Engineering, Nanyang Technological University, Singapore, as a Senior Lecturer, where he has been an Associate Professor since 1999 and the Deputy Head of Power Engineering Division from 2008 to 2014. His current research interests include microgrid energy management systems, electricity markets, spinning reserve, energy storage, and renewable energy sources.